

## Article

# Definition of a Protocol for the Experimental Monitoring of Rising Damp in Three Different Masonry Models with Tuff, Carparo, and Lecce Stone

Paolo Maria Congedo <sup>1</sup>, Cristina Baglivo <sup>1,\*</sup>, Giovanni Quarta <sup>2</sup>, Pasquale Di Gloria <sup>1</sup>  
and Delia D'Agostino <sup>3</sup>

<sup>1</sup> Department of Engineering for Innovation, University of Salento, 73100 Lecce, Italy; paolo.congedo@unisalento.it (P.M.C.); pasquale.digloria@unisalento.it (P.D.G.)

<sup>2</sup> ISPC-CNR (The Institute of Heritage Science), 73100 Lecce, Italy; giovanniquarta@cnr.it

<sup>3</sup> Joint Research Centre (JRC), European Commission, 21027 Ispra, Italy; delia.dagostino@ec.europa.eu

\* Correspondence: cristina.baglivo@unisalento.it

**Abstract:** This work presents a new protocol for monitoring rising damp, which is applied to three masonry models made of tuff, carparo, and Lecce stone. First, the physical characteristics of each stone were derived in the laboratory, which included porosity, imbibition, drying index, permeability, capillarity, and sorptivity. In this case, the protocol provided three columns, one for each material, consisting of five blocks. A layer of cotton tissue was interposed between columned blocks to simulate the hygroscopic behavior of a mortar, allowing a quick disassembly and reassembly of the multiblock columns for a quick weighing. The bottoms of the columns were immersed in water to a level of about three centimeters, providing a constant replenishment for the phenomena of evaporation and rising in the stone. The maximum height achieved by the rising damp depends on the characteristics of the building materials, i.e., the amount and size of pores, pore connectivity, etc. Since these materials have different physical characteristics, the objective was to quantify the rising moisture level of the three materials tested, block by block, in a controlled indoor microclimate environment. The three columns were periodically weighed, the quantity of collected water was evaluated, and a thermographic survey was performed. The results show that at the end of the test, the highest level of rising damp is reached by tuff with a height of 43 cm, followed by Lecce stone and carparo with a height of 40 cm and 21 cm, respectively. The innovation of this study is the proposal of a new flexible and easy-to-apply method for monitoring this phenomenon. It gives clear and numerically comparable results. Moreover, it is applicable to any type of stone, allowing the user to evaluate both the existing state and different design solutions.

**Keywords:** rising damp; building stones; thermography; moisture; carparo; tuff; Lecce stone; experimental data; capillarity; evaporation



**Citation:** Congedo, P.M.; Baglivo, C.; Quarta, G.; Di Gloria, P.; D'Agostino, D. Definition of a Protocol for the Experimental Monitoring of Rising Damp in Three Different Masonry Models with Tuff, Carparo, and Lecce Stone. *Energies* **2022**, *15*, 892. <https://doi.org/10.3390/en15030892>

Academic Editor: Shi-Jie Cao

Received: 20 December 2021

Accepted: 22 January 2022

Published: 26 January 2022

**Publisher's Note:** MDPI stays neutral with regard to jurisdictional claims in published maps and institutional affiliations.



**Copyright:** © 2022 by the authors. Licensee MDPI, Basel, Switzerland. This article is an open access article distributed under the terms and conditions of the Creative Commons Attribution (CC BY) license (<https://creativecommons.org/licenses/by/4.0/>).

## 1. Introduction

Over the years, buildings must undergo a lot of maintenance operations [1]. Several causes can lead to damage to the building stock, and numerous interventions can be implemented to anticipate or reduce the negative effects [2,3]. For example, damage to buildings can be caused by impending climate change, i.e., buildings designed without considering the rise in outdoor temperatures over the years [4]. In addition, the development of new technologies has led to the design of increasingly insulated and sealed buildings, and this can lead to moisture problems on the walls if the openings, considered the most delicate element of the building, are not designed properly [5] or if there are no mechanical ventilation systems. The presence of humidity can lead to buildings that are increasingly less comfortable and that require numerous interventions to improve their healthiness.

The problem of controlling and eliminating moisture from masonry is one of the most crucial points in the maintenance of buildings [6]. Degradation caused by humidity involves both aesthetic and hygienic-sanitary problems. Damage caused by moisture can be both visible and invisible, since, in addition to moisture stains and cracking of plasters, the structure of masonry layers can deteriorate [7].

Rising damp is an important cause of damage and deterioration in historic buildings [8]. It depends mainly on the subsoil water and some characteristics of the construction materials such as the porosity. Rising damp negatively affects the mechanical and thermal behavior of materials, and it can also affect the preservation of monument decorations, air quality, and the well-being of occupants [9]. Despite its importance, rising damp is rarely considered as compared with, for example, seismicity risk and energy efficiency, for which measures and policies are in place. Furthermore, remedial actions that are taken are sometimes ineffective.

Different processes are simultaneously involved in rising damp. Due to the physics and chemistry interactions, the study and prediction of this phenomenon is very challenging [10]. Causes of deterioration may be related to the nature of the materials and their exposure to degrading agents, or due to design inaccuracies. For this reason, the study of material degradation becomes a crucial step in the retrofit of existing buildings [6].

The control of dampness performance in buildings has been a subject of growing importance in recent years [11]. It has been noted that a lack of knowledge regarding the propagation of the phenomenon has led to inadequate corrective measures that, in the worst cases, have accelerated the phenomenon [12]. The literature [13,14] has emphasized that knowledge of the dynamic trend of the phenomenon is fundamental for the conservation of historical heritage. It has been determined [15] that alternating wetting and drying has an impact on water transport within construction. Capillary rise going from the bottom to the top of materials is a physical process determined by capillary properties. The subsoil contact and condensation of air moisture also influence the process. Due to infiltration, indoor comfort can be lost, and materials degraded [16,17]. The capillarity process also carries soluble salts from the ground [18] that can lead to crystallization, which contribute to material degradation [19,20]. This process is exacerbated when the sorption of water, which conveys soluble salts, is not adequately compensated for by indoor evaporation. Water works as a vector for salts dissolved in a solution by carrying them upward [21]. Salts crystallize inside the pores, both in the outer (plaster) and inner layers (walls). This process saturates the pores, leading to swelling, detachment, and surface degradation phenomena. The inherent characteristics of a masonry to retain moisture, as well as the microclimatic conditions of the site influence this process [22].

There are many tools that have been used to calculate this phenomenon, but they are complex and require a large amount of information, which commonly prevent their application [23]. A monitoring campaign can be useful to obtain the data required in water transport modeling. The use of simplified models can approximate the phenomenon with good accuracy and parameter estimations [7].

In this paper, a methodology has been developed for the analysis of rising damp applied to different masonries using different stones. The maximum height reached by moisture depends on the building properties and its composing elements as well as the porosity, the connections among pores, etc. The goal is to develop a new methodology to quantify the level of rising damp in a controlled microclimate environment. The method is new and easily applicable to different types of materials.

## 2. Preliminary Data: Stone Characterization

### 2.1. Imbibition Coefficient

The test for the calculation of the imbibition coefficient was carried out following the standard UNI EN 13755 [24]. The standard suggests using at least 3 cubic samples, with 5 cm sides, to derive the water absorption by immersion at the atmospheric pressure. The assessment is considered completed when the difference between two consecutive

weighing, within 24 h, is up to 0.1% of the first of the two masses. The detailed calculation procedure has been proposed in a previous study [6]. The water absorption in the sample ( $A_b$ ) is derived as:

$$A_b = \frac{m_s - m_d}{m_d} \cdot 100 \quad (1)$$

where  $m_s$  is the saturated sample mass relative to the last weighing and  $m_d$  is the dry mass of the specimen, relative to the first weighing.

The imbibition coefficients obtained from the arithmetic mean of all the samples for each material are shown below:

- (1) Lecce stone, 14.95%;
- (2) Carparo, 20.42%;
- (3) Tuff, 29.46%.

## 2.2. Drying Index

The drying index determination was performed following the standard UNI EN 16322 [25]. According to the standard, at least 3 cubic samples, with 5 cm sides, are used. This test investigates the drying capacity of inorganic porous materials. The test ends when the sample's final mass ( $m_f$ ) does not change within two successive weighings. The detailed calculation procedure has been proposed in a previous study [6]. Recordings were made with an interval of 10 min during the first hour, then, every hour during the following 7 h, and then, twice a day with an interval of 6 h between two measurements. To obtain the drying curve, the amount of residual water in the sample per unit area ( $\text{kg}/\text{m}^2$ ) at the time ( $t_i$ ) is calculated as:

$$M_i = \frac{m_i - m_f}{A} \quad (2)$$

where  $m_i$  is the initial mass at time  $t_0$ ,  $m_f$  is the final mass, and  $A$  is the exchange surface area.

The calculation of  $M_i$  values is reported as a function of time expressed in hours.

The drying index is calculated using the following formula:

$$ID = \int_0^f \frac{M_i dt}{M_{max} t_f} \quad (3)$$

where  $M_{max}$  is the maximum mass and  $t_f$  is time related to maximum mass.

The drying index values obtained from the arithmetic mean of all the samples for each material are shown below:

- (1) Lecce stone, 0.06185;
- (2) Carparo, 0.06920;
- (3) Tuff, 0.08305.

## 2.3. Permeability

The Normal 21/85 [26] is the reference standard to derive permeability, expressed in  $\text{g}/\text{m}^2 \times 24 \text{ h}$ , using at least three samples of dimensions  $5 \times 5 \times 1 \text{ cm}$ .

This test characterizes the material by determining the water vapor that flows per unit area under stationary conditions in the unit of time. It considers a material of a given thickness and the difference in partial pressure of water vapor between two parallel surfaces.

The test ends when a steady state is reached and the difference between two successive weighings, within 24 h, is lower than 5%. The detailed calculation procedure has been proposed in a previous study [6] and is as follows:

$$\frac{(\Delta M_i - \Delta M_{i-1}) \cdot 100}{\Delta M_i} \leq 5\% \quad (4)$$

To derive the permeability, the arithmetic average of the weight variations at least within three time intervals (during which the  $\Delta M$  had fluctuations around a mean) was

calculated. The mean value was, then, calculated for each samples set. The permeability to water vapor, thus calculated, is expressed in  $\text{g}/\text{m}^2 \times 24 \text{ h}$ , at  $20^\circ\text{C}$ . As our test was carried out at  $23^\circ\text{C}$  (different, therefore, from  $20^\circ\text{C}$ ), the experimental value was adjusted as follows:

$$\text{Perm}_{20^\circ\text{C}} = \text{Perm}_{t_x} \cdot \frac{p_{20^\circ\text{C}}}{p_{t_x}} \quad (5)$$

where  $p_{(20^\circ\text{C})}$  is the partial vapour pressure at  $20^\circ\text{C}$  and  $p_{(t_x)}$  is the partial vapour pressure at the test temperature.

Table 1 shows the results for Lecce stone, carparo and tuff corrected with Equation (5).

**Table 1.** Vapor permeability of Lecce Stone (L.S.), carparo (C.) and tuff (T.).

Specimen	Area ( $\text{m}^2$ )	Average ( $\Delta M_2$ , $\Delta M_3$ , $\Delta M_4$ ) (g)	Perm <sub>(20°)</sub> ( $\text{g}/\text{m}^2 \cdot 24 \text{ h}$ )	Average Perm <sub>(20°)</sub> ( $\text{g}/\text{m}^2 \cdot 24 \text{ h}$ )
1 L.S.	0.0016	0.392	202.540	<b>192.761</b>
2 L.S.	0.0016	0.378	195.462	
3 L.S.	0.0016	0.332	171.645	
4 L.S.	0.0016	0.385	199.113	
5 L.S.	0.0016	0.378	195.048	
1C.	0.0016	0.582	300.890	<b>326.047</b>
2C.	0.0016	0.542	280.225	
3C.	0.0016	0.573	295.931	
4C.	0.0016	0.580	299.771	
5C.	0.0016	0.878	453.419	
1T.	0.0016	0.759	392.198	<b>373.416</b>
2T.	0.0016	0.755	390.097	
3T.	0.0016	0.640	330.408	
4T.	0.0016	0.721	372.307	
5T.	0.0016	0.740	382.072	

#### 2.4. Capillarity

This test refers to the standard UNI EN 15801 [27] which foresees the use of at least 3 samples of dimensions  $5 \times 5 \times 2 \text{ cm}$ . The aim of the test is to derive the water absorption by capillarity. The test ends when the difference between two consecutive weighings within a 24 h interval is less than 1%. The detailed calculation procedure has been proposed in a previous study [6].

The time interval of the successive weighings is a function of the water absorption speed. The first measurements are taken at close intervals that we identified at 5 min for the first 30 min, then 15 min, then 1 h, and finally 24 h.

The amount of water absorbed at time  $t_i$  per unit area  $Q_i$  is derived using:

$$Q_i = \frac{m_i - m_0}{A} \quad (6)$$

where  $m_0$  is the dry sample mass.

The  $Q_i$  average values are derived for each series and reported on the capillary absorption curve (Figure 1) as a function of the square root of time  $t_i^{1/2} (\text{s}^{1/2})$ .

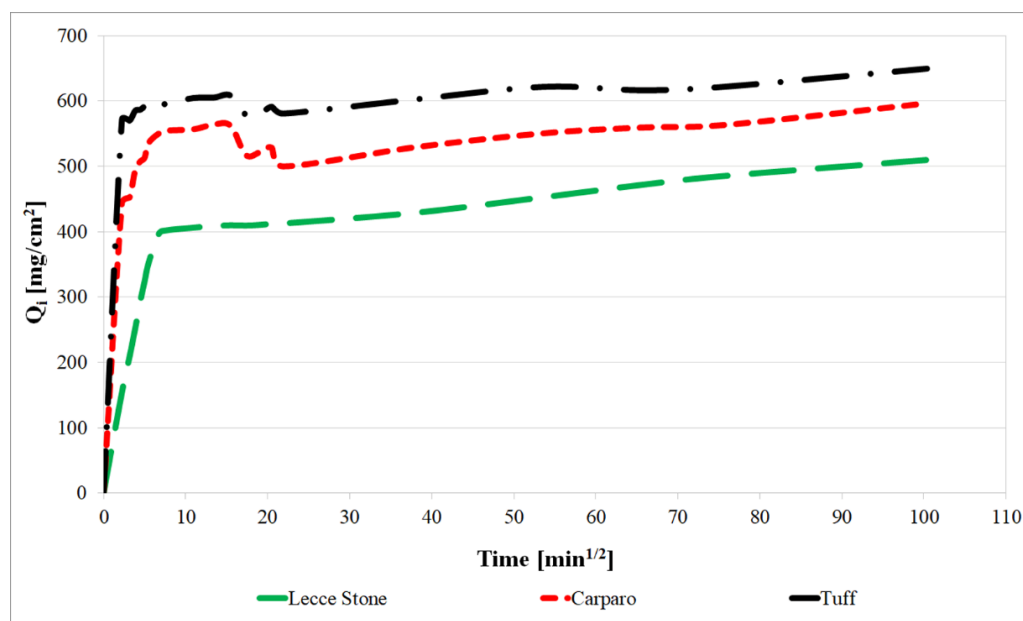


**Figure 1.** Development of capillary rising coefficient of the three materials.

### 2.5. Sorptivity

A material can absorb and transmit water and other liquids by capillarity depending on its sorptivity. To derive this property, the results were obtained from the capillary rising coefficient test [6].

The first part of the curve in Figure 1 is selected (in this case the first nine measurements are considered) because it best describes the unknown property. Through the trend line, the equations of the curves in Figure 1 are traced as follows:

- Lecce stone,  $y = 0.6026x + 2.6269$ ;
- Carparo,  $y = 0.6118x + 1.8726$ ;
- Tuff,  $y = 0.5415x + 0.3195$ .

From the trend lines, it was also possible to identify through the intercept, the sorptivity (S) value sought, as shown below:

- Lecce stone,  $0.3195 \text{ mm}/\text{min}^{\frac{1}{2}}$ ;
- Carparo,  $1.8726 \text{ mm}/\text{min}^{\frac{1}{2}}$ ;
- Tuff,  $2.6269 \text{ mm}/\text{min}^{\frac{1}{2}}$ .

## 3. The Protocol Definition

This section illustrates the protocol proposed for monitoring rising damp in the laboratory. First, the instruments used for monitoring are reported, as well as the procedures for the installation of specimens. The protocol is divided into two main phases:

- Experimental phase n.1, in which the effects on capillarity in the initial transition phase are observed.
- Experimental phase n.2, in which the effects on capillarity in the regime phase are analyzed.

### 3.1. Measurement Equipment

A Scale House DHS 150K dynamometer was used for the experimental test, whose technical specifications are summarized in the Table 2.

**Table 2.** Technical specifications of the dynamometer.

Model	Capacity (kg)	Division (g)	Min. cap. (kg)
DHS 150 K	150	50	1
Power supply	3 × 1.5 V AA battery. Low energy consumption, designed for lengthening the battery life (150 battery life). “Auto-off” function after the set time: 0, 5, 15, 30, and 60 min.		
Zero range	Within the configured percentage: ±0, 2, 4, 10, 20, and 50% of maximum load capacity		
Zero tracking	0,5 e/s		
Auto zero start-up	Within the configured percentage: ±0, 2, 4, 10, 20, and 50% of maximum load capacity		
Display	LCD with 5 digit		
Operative temperature	−10 °C to +40 °C		
Relative humidity	≤90% at 20 °C		

For the experimental test, a Flir ThermoCAM B20 thermal imaging camera was used. The principal characteristics are a spectral field from 7.5 to 13  $\mu\text{m}$ , a thermal resolution less than 0.08 °C at full frequency of 50 Hz, a temperature measuring range from −40 °C to +55 °C, and a precision of  $\pm 2\text{ °C} \pm 2\%$  of range.

A datalogger was used to measure temperature, humidity, and dew point (Table 3).

**Table 3.** Datalogger data sheet.

<b>Temperature</b>	<b>Accuracy (overall error)</b>	0.45 °C (1.04 °F) typical (5 to 60 °C)
	<b>Long term stability</b>	<0.02 °C (0.04 °F)/year
	<b>Measurement range</b>	From −35 to 80 °C (from −31 to 176 °F)
	<b>Internal resolution</b>	0.5 °C (1 °F)
<b>Relative Humidity</b>	<b>Accuracy (overall error)</b>	3% RH (20 to 80% RH)
	<b>Long term stability</b>	<0.25% RH/year
	<b>Measurement range</b>	0 to 100% RH
	<b>Internal resolution</b>	0.5% RH
<b>Dew Point</b>	<b>Accuracy (overall error)</b>	1.7 °C typical (From −35 to 80 °C and from 40 to 100% RH)
	<b>Dimensions</b>	108 × 25 × 22 mm (4.25 × 0.98 × 0.86")
	<b>Readings</b>	16,382 temperature, 16,382 relative humidity
	<b>Operating temperature range</b>	From −35 to +80 °C (from −31 to +176 °F)
	<b>Logging rate</b>	User selectable between 10 s and 12 h

### 3.2. Experimental Setup

1. The experimental setup involves the use of two wetting tanks with three columns each, one for each stone used. Each column consists of five blocks of size 20 × 20 × 20 cm<sup>3</sup>. The first three columns undergo the weighing procedure, the other three remain unperturbed and undergo the same wetting procedure as the first ones. The contact between the blocks is made with a suitable absorbent material (cotton fabric) to ensure a good contact surface and to simulate the hydric behavior of the mortar (Figure 2). Although mortar has been found to counteract rising damp [28,29], this study aims to monitor a base case, where all properties can be subsequently modified.

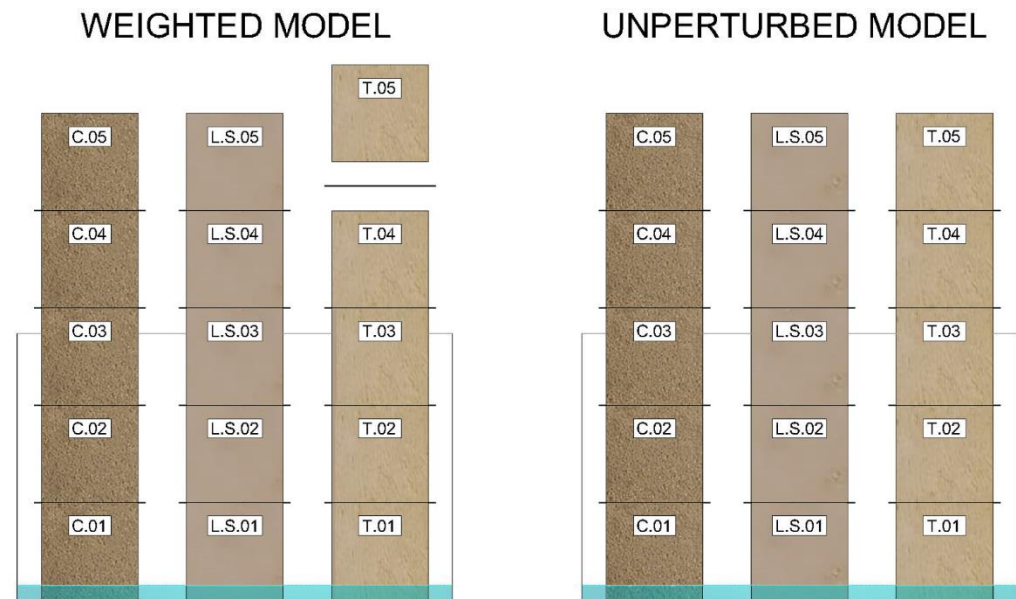


**Figure 2.** Experimental setup.

2. The blocks are numbered from bottom to top and preliminarily weighed; this operation allows for the weighing process to proceed regularly for the determination of the water absorbed at different heights.
3. The cotton tissues are numbered from bottom to top to reposition them in the same level after the weighing operation and, therefore, to disrupt the pre-weighing conditions as little as possible.
4. Blocks are positioned in a tank to allow wetting of the lower base of each column. An indication system (mark on the block at 3 cm height) of the immersion level of the column base is provided, which is the level that must be the same for all the columns.
5. Columns should be placed with the base in the dry tank for 24 h in advance to acclimatize and stabilize the surface temperature.
6. The datalogger is placed close to the columns to strictly control the microclimatic conditions at the boundary.

### 3.3. Experimental Phase n.1: Effects on Capillarity in the Initial Transition Phase

The goal of this phase is to analyze the phenomenon on the column initially dry, that is, wetted at the bottom with tap water having a low concentration of salts. This represents the starting point for time measurement. Water characterization data carried out by the Apulian Aqueduct [30].

In this phase, qualitative and quantitative data regarding the rise of water in the columns are collected. This involves continuous monitoring together with thermographic reports that provide the framework of the water movement inside the columns and weighing at defined time intervals.

Table 4 shows the time frame to be observed for weighing, thermography (IR), and wetting tests.

**Table 4.** Time frame for weighing steps, thermography (IR) and wetting tests.

Day	Time	Weighing	Ir	Water Refilling	Experimental Phase
1	Starting point	X	X	X	Initial Transition Phase
	0:15		X		
	0:30		X		
	0:45		X		
	1:00		X		
	1:30		X		
	2:00		X		
	3:00		X		
	4:00		X		
	5:00		X		
	6:00		X		
	7:00		X		
	8:00		X		
9:00		X			
10:00		X			
2	One measure per day	X	X	X	Regime Phase
3	One measure per day		X	X	
4	One measure per day		X	X	
5	One measure per day		X	X	
6	One measure per day		X	X	
7	One measure per day	X	X	X	
14	One measure per day	X	X	X	
21	One measure per day	X	X	X	
28	One measure per day	X	X	X	
Every two weeks	One measure per day	X	X	X	

### Executive Modalities For Thermographic Tests

1. The first thermal image is acquired before adding water to the tank.
2. For the camera setting ( $T^{\circ}\text{C}/\text{RH}$  in %), the value defined by the datalogger is used as a reference.
3. The thermal imaging camera is positioned in front of the columns for real-time rising damp monitoring.
4. Since the phenomenon is very rapid at the beginning, and then it slows down and stabilizes, a time cadence is fixed for the succession of thermograms, as shown in Table 4.
5. Water replenishment in tanks when the water level deviates from the initial reference value.
6. All steps from 2 to 5 are repeated periodically for the entire duration of the experiment which, it is recommended, should not be less than one year. After an initial transient period with an extremely rapid rising phenomenon, there is a period of stabilization of the phenomenon with limited temporal variations. Therefore, the periodicity of the thermographic recordings can be frequent in the first period, and then reduce afterward.

### 3.4. Experimental Phase n.2: Effects on Capillarity in Regime Phase

The objective of this phase is the analysis of rising damp starting from the regime phase situation previously reached (flow of capillary rise in the sample columns already stabilized).

In this phase, the quantitative data related to the weight variation of the blocks continue to be collected by repeating the weighing of the various blocks at defined time intervals, from which the percentage increase in the weights of the blocks as compared with the initial weights are obtained. Before each weighing, i.e., before the disassembly of the various blocks, a thermographic recording of all the columns is carried out. At the end of weighing, the columns are immediately reassembled, respecting the order of disassembly.

#### Executive Modes for Weighing Tests

1. Setting of the camera ( $T^{\circ}\text{C}/\text{RH}$  in %) taking as reference the average value coming from the two dataloggers and execution of the thermogram of the entire columns.
2. Disassembly, and immediate weighing, of the various blocks making up the columns, proceeding from top to bottom.
3. Reassembly of the various blocks immediately after completion of weighing operations, taking care to reposition the blocks in the exact starting order.

#### 4. The Case Studies

The case study setting does not perfectly match the previously proposed procedure. This is because it was the case study itself that suggested a number of adjustments that allowed the proposed methodology to be refined.

Six columns were constructed, two for each material (one for tank), each consisting of five blocks, with a cotton fabric state interposed between each block (Figure 3). Each block has a size of  $20 \times 20 \times 20$  cm, while the cotton fabrics measure  $23 \times 23 \times 0.1$  cm. All blocks have been labeled with a code, carparo (C.), Lecce stone (L.S.), and tuff (T.), the numbering respects the arrangement of the blocks, increasing from the bottom to the top. The labeling of blocks and textiles simplified the repositioning of blocks and textiles in their original position after each weighing operation. The test was conducted by placing the blocks inside a tank, measuring  $90 \times 60 \times 55$  cm.



**Figure 3.** From left to right: carparo (C.), Lecce stone (L.S.), and tuff (T.).

Initially, once the blocks were positioned in the tank, they were left to dry for 24 h, to allow the achievement of thermodynamic equilibrium with the surrounding environment, and thus, to allow the achievement of the physiological mass ( $m_f$ ) of the various blocks.

Subsequently, the basins were filled with water. The monitoring was carried out starting from the initial moment when the specimens were dry, and water was added for the first time into the basin. A periodic replenishment of water in the basin, to maintain a constant level of immersion of the base of the columns (about 3 cm), was done by using a 5 L tank. By weighing the blocks periodically, the wet mass ( $m_u$ ), and thus, consequently, the percentage of water absorbed  $U_f$  at different heights, was determined using Equation (7):

$$U_f = \frac{m_u - m_f}{m_f} \cdot 100 \quad (7)$$

Through continuous monitoring, based on a combination of visible and thermographic shots and weighing at defined time intervals, it was possible to obtain qualitative and quantitative results of the water propagation inside the columns. The monitoring period was from 6 September 2018 to December 2018.

Specifically, on September 6 the dry specimens were placed inside the basin, exactly 24 h before the start of the measurements. Then, after 24, the first weighing was performed on 7 September, to detect the physiological mass of the dry specimens. Then, after the weighing operations and having repositioned the various specimens, the basin was filled with water. After two hours, the first thermographic images were acquired. From 7–14 September, weighing operations of the wet specimens were performed weekly, from 14 September 2018 to 21 December 2018, bi-weekly.

Table 5 shows the dates and the quantity of water supplies during the analysis period.

**Table 5.** Water replenishment.

Date	Quantity [l]
7 September 2018	20
14 September 2018	5
21 September 2018	5
28 September 2018	5
5 October 2018	5
12 October 2018	5
26 October 2018	10
9 November 2018	10
23 November 2018	10
7 November 2018	10
21 November 2018	10

## 5. Results and Discussion

The tests have shown, although in different ways for the three materials, two distinct phases, namely a transient phase and a stabilized phase. In the first phase, an initial rapid increase in moisture was observed, which then slowly decreased over time until a stabilized phase was reached in which the upward flow in the columns stabilized at a certain height. This can be observed by plotting the absorption curves in terms of weight, moisture, and rise height. The trends depend on the type of material, the constancy of the water supply, the microclimate, and the multiblock configuration instead of monoblock columns.

### 5.1. Weight-Time Absorption Curves

The weight-time absorption curves represent the weight variation as a function of time, due to water absorption in the blocks of each column. Table 6 shows the results of the weighing tests performed on all blocks.

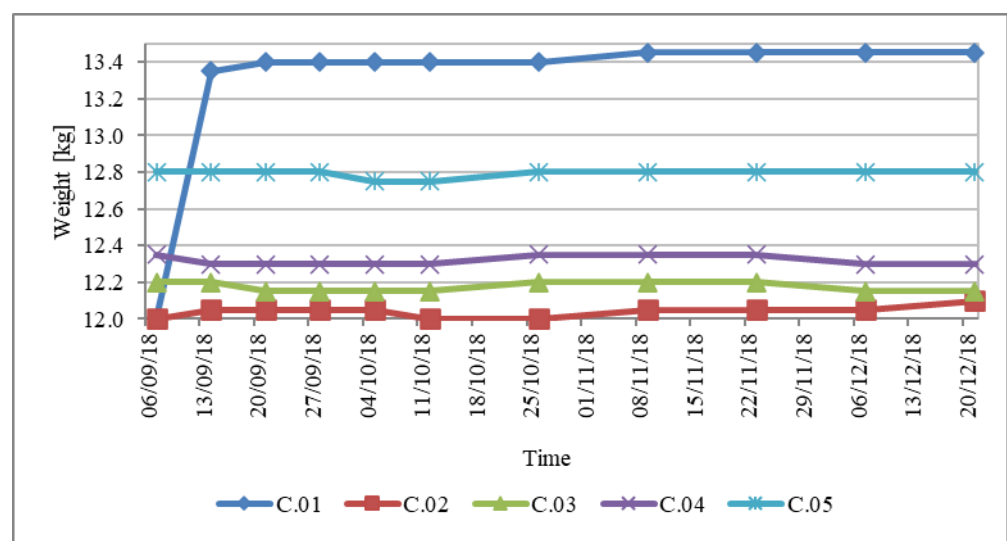
**Table 6.** Weighing data of the three blocks, from 7 September to 21 December.

Blocks	Block Weighing (kg)										
	07/09	14/09	21/09	28/09	05/10	12/10	26/10	09/11	23/11	07/12	21/12
C.01	12.00	13.35	13.40	13.40	13.40	13.40	13.40	13.45	13.45	13.45	13.45
C.02	12.00	12.05	12.05	12.05	12.05	12.00	12.00	12.05	12.05	12.05	12.10
C.03	12.2	12.2	12.15	12.15	12.15	12.15	12.2	12.2	12.2	12.15	12.15
C.04	12.35	12.3	12.3	12.3	12.3	12.3	12.35	12.35	12.35	12.3	12.3
C.05	12.8	12.8	12.8	12.8	12.75	12.75	12.8	12.8	12.8	12.8	12.8
L.S.01	13.55	15.3	15.3	15.3	15.35	15.35	15.35	15.35	15.7	15.6	15.75
L.S.02	14	14.05	14.15	14.15	14.25	14.3	14.3	14.3	14.6	14.6	14.6
L.S.03	13.55	13.55	13.55	13.55	13.55	13.55	13.55	13.5	13.6	13.6	13.6
L.S.04	13.55	13.55	13.55	13.55	13.55	13.55	13.55	13.55	13.55	13.55	13.55
L.S.05	13.55	13.55	13.55	13.55	13.55	13.55	13.55	13.55	13.55	13.55	13.55
T.01	10.9	13.55	13.6	13.65	13.65	13.7	13.7	13.7	13.7	13.7	13.8
T.02	11.05	11.1	11.1	11.2	11.6	12.8	12.8	12.8	13	13.1	13.4
T.03	10.95	10.95	10.95	10.95	10.95	11	11.1	11.1	11.1	11.1	11.1
T.04	11.15	11.15	11.15	11.1	11.1	11.15	11.15	11.15	11.15	11.15	11.1
T.05	11.35	11.35	11.35	11.35	11.35	11.35	11.35	11.3	11.35	11.35	11.35

Figures 4–6 show the trends of weight-time absorption for carparo, Lecce stone, and tuff.

All the graphs show, although in different ways, in the first two blocks, a considerable increase in initial weight, with a high slope, and therefore, with considerable rapidity; this occurs because they are in direct contact with the water for part of their height. Moving on to the blocks immediately above, the phenomenon is not emphasized as in those closer to the water basin, because the absorption comes from the block below.

Considering the carparo, the first measurement of the first block (C.01) shows an increase in weight of 1.35 kg, while the increase in the second block (C.02) is 0.5 kg, after which both go towards a stabilization of weight, which is reached on November 9 for the first block (eighth weighing) and after the first weighing for the upper blocks. The difference between the last and first weighing of the first block (C.01) shows an increase in weight of 1.45 kg. Carparo stone immediately accumulates the amount of water and stabilizes in weight.

**Figure 4.** Weight-time absorption curves for the carparo column (C).

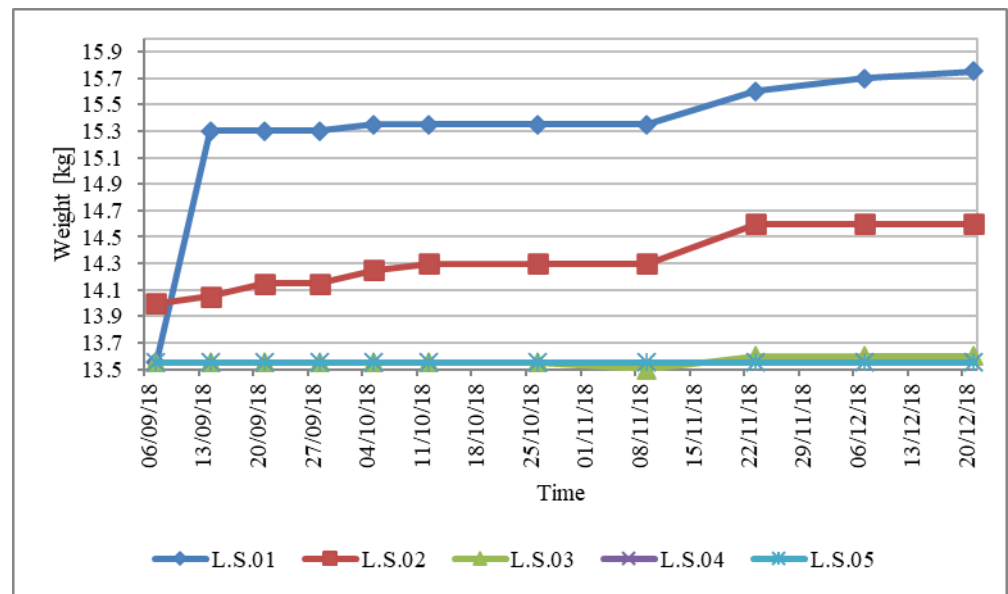


Figure 5. Weight-time absorption curves for the Lecce stone column (L.S.).

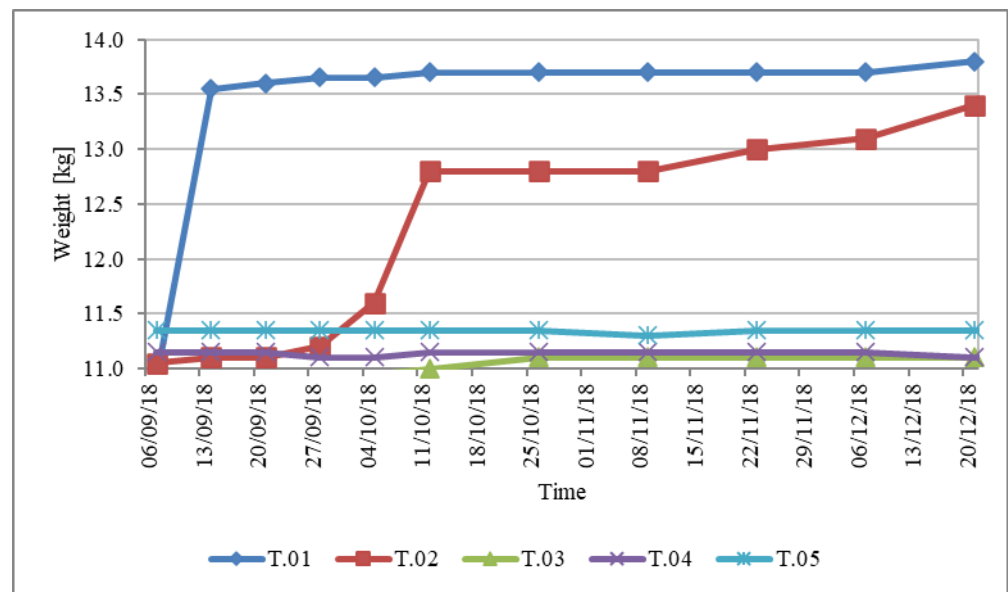


Figure 6. Weight-time absorption curves for the tuff column (T.).

As regards the Lecce stone, the first measure of the first block (L.S.01) shows an increase in weight of 1.75 kg. Lecce stone shows a more gradual trend than carparo, reaching a higher final weight. The final total weight in the last weighing increased in the Lecce stone (L.S.01) by 2.2 kg as compared with the first weighing. As compared with carparo, whose second block finds an immediate stabilization, Lecce stone shows a higher and gradual growth also in the second block (L.S.02).

Tuff achieves the highest weight. Indeed, the weight increase in the first weighing of the first block is already high, equal to 2.65 kg (greater than the total increase for the carparo and Lecce stone), and the final total weight is increased by 2.9 kg. As compared with the other two stones, tuff has a change in weight in both the second and third block (T.03).

The mesopores present in the tuff facilitate the capillary rise phenomena, while the low increase in weight of the carparo is due to the high percentage of macropores that do not facilitate capillary rise. In the Lecce stone, as in the tuff, there is an initial increase in weight; however, whereas in tuff the increase is almost instantaneous, in Lecce stone it is

protracted in time. This is due to the presence of very small pores inside the Lecce stone. In general, the smaller the capillaries, the more they tend to absorb moisture, retaining it. The same very thin capillaries, however, greatly hinder the movement of moisture within them, making it very slow.

As for the blocks in levels 3, 4, and 5, the trend has been almost constant from the beginning, because the increase in water involved only the blocks at the base and those immediately above.

### 5.2. Humidity-Time Absorption Curves

This section shows the percentage of water absorbed  $U_f$  (calculated by Equation (7)) as a function of time, referring to the first two blocks of the columns, in relation to carparo (Figure 7), Lecce stone (Figure 8), and tuff (Figure 9). The physiological mass ( $m_f$ ) for each of the three materials was recorded on 7 September 2018. The amount of water absorbed is greater in tuff, a phenomenon due to its high porosity. The phenomenon is also clearly evident in the second block of tuff (T.02), which is significantly impacted by the presence of water coming from the previous block (T.01). The second block of Lecce stone (L.S.02) also shows a gradual increase in the percentage of water in it, but less than the tuff (C.02). The second block of carparo (C.02) is less influenced by capillary rise, in fact it shows a constant trend, with a very low percentage of water inside.

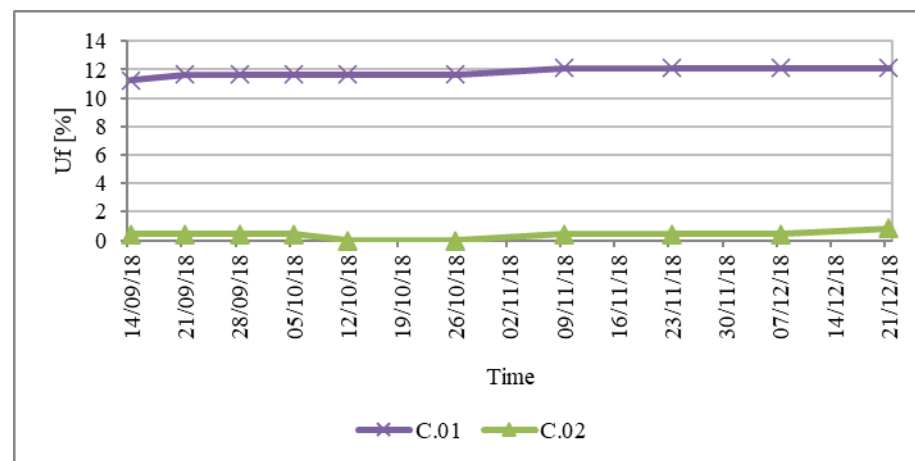


Figure 7. Moisture-time absorption curves for carparo blocks (C.).

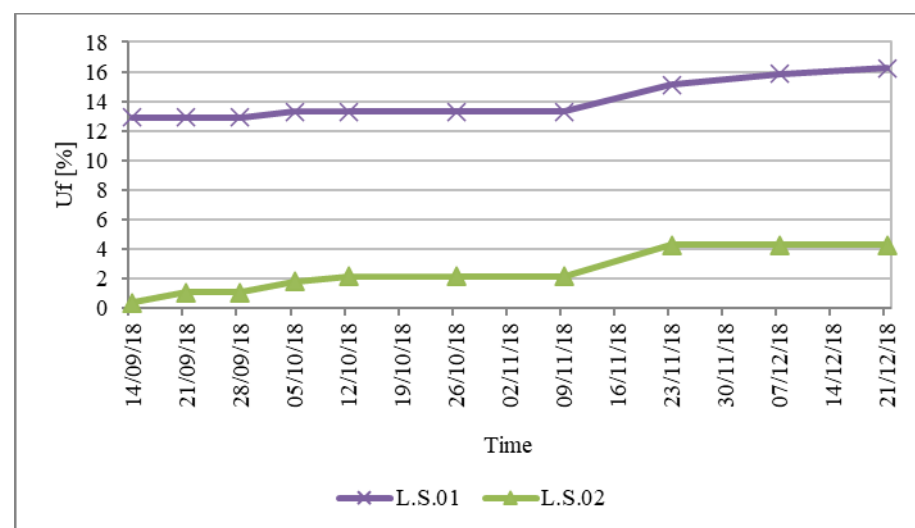
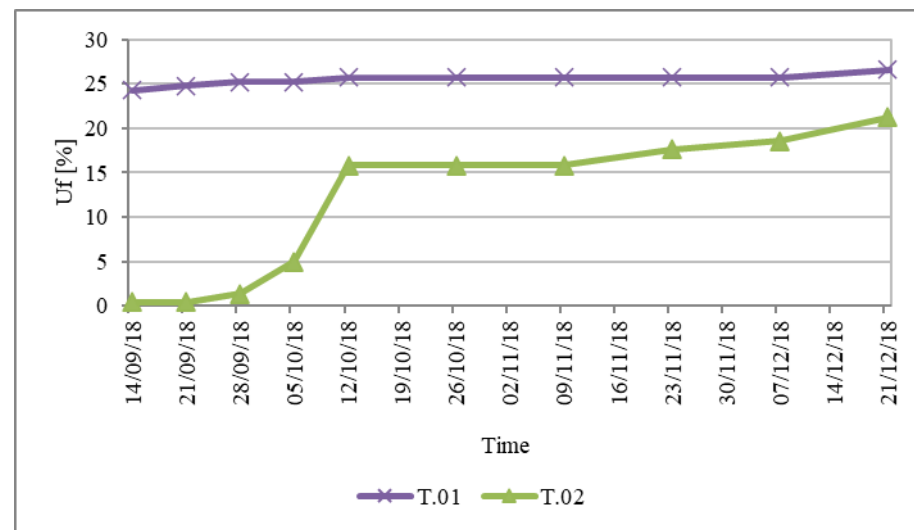


Figure 8. Moisture-time absorption curves for Lecce stone blocks (L.S.).



**Figure 9.** Moisture-time absorption curves for tuff blocks (T).

### 5.3. Rising Height-Humidity Absorption Curves

Figure 10 shows the variation of the rising height as a function of time for the columns in carparo, Lecce stone, and tuff. Thermographic images presented in Appendix A were used to measure rise heights. The previous observations were confirmed by the data on the height of rising damp.

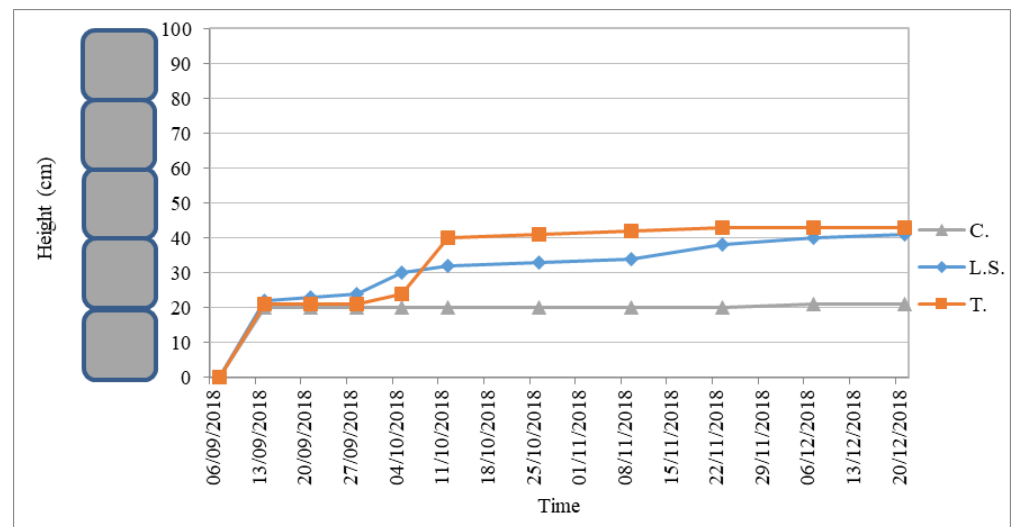


**Figure 10.** Ascent height-time absorption curves for carparo (C.), Lecce Stone (L.S.), and tuff (T.).

Looking at Figure 10, all three materials are strongly affected by rising damp, in fact, there is an exponential increase in the height of rising damp from the first day.

Starting from the base of the columns, it can also be seen that the rising damp has completely involved the first two blocks of Lecce stone (L.S.) and tuff (T.) and that it has completely involved only the first block of carparo (C.).

In the three materials, the following asymptotic values of ascent height were reached:

- 21 cm for carparo;
- 40 cm for Lecce stone;
- 43 cm for tuff.

For carparo and tuff, the final ascent height is reached in a short time (faster in carparo), while for Lecce stone, it is reached more slowly.

This is due to the different types of porosity and, therefore, to the different kinetics of absorption. Tuff and carparo are characterized by larger pores than those of Lecce stone, therefore, while tuff and carparo have an easy and rapid absorption of water, Lecce stone has a rapid intake in the initial phase but prolonged over time.

#### 5.4. Thermographic Report

The rising phenomenon in the three materials tested was monitored quantitatively and qualitatively through the acquisition of photographs and infrared thermographic images. Figure 11 shows an example of the thermographic image, the complete report is presented in Appendix A.

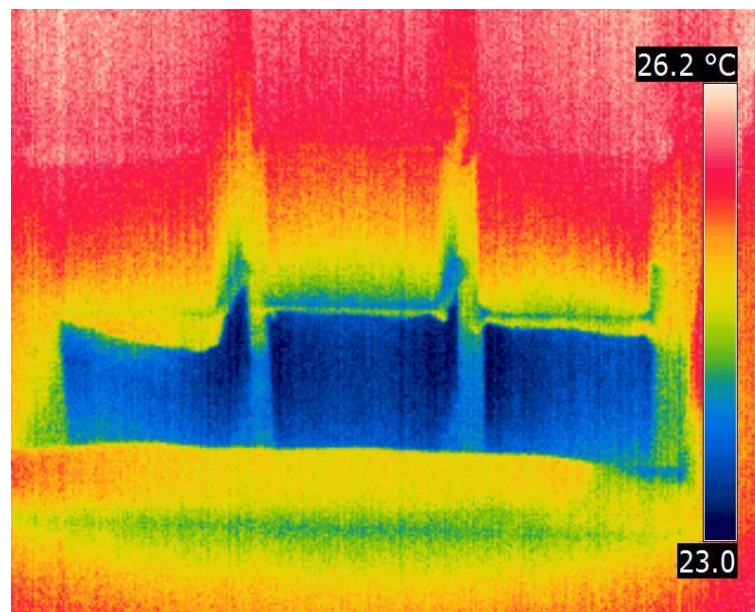


**Figure 11.** Thermographic report dated 14 September 2018 for carparo (C.), Lecce stone (L.S.), and tuff (T.).

More specifically, this occurred before weigh-in operations from 14 September to 21 December 2018.

As specified previously, on 7 September 2018, approximately two hours after first filling the tanks with water, IR photos were taken to monitor the situation. In these first two hours, the three materials immediately absorbed water and reached the following heights:

- 13 cm in the carparo column;
- 8 cm in the Lecce Stone column;
- 14 cm in the tuff column.

Therefore, from the initial stages, the upward trend occurred, i.e., fast absorption for tuff and carparo and slow absorption for Lecce stone.

## 6. Conclusions

This study starts from the awareness that the presence of moisture in masonry is responsible, in the short and long term, for the presence of serious pathologies in a building, which can impact the safety, health, and comfort of the occupants. It is well known that rising damp leads to a degradation of the building material due to chemical interactions with water and salts dissolved inside the masonry.

This study proposes a new protocol for monitoring the phenomenon of rising damp in masonry in the laboratory. These guidelines are easily applicable and flexible, as they can be applied for any material.

To highlight the effectiveness of the proposed guidelines, the analysis of a case study is proposed, monitoring the phenomenon on three different types of stones, namely carparo, Lecce stone, and tuff. The choice of these materials is not casual as they are the materials most used in South-Eastern Italy, where the phenomenon of rising damp is present in a very strong way, and impacts the comfort of occupants, especially, on the ground floors of buildings. These are local materials, easily available in local caves, but characterized by a very high degree of sensitivity to water. According to the protocol, three columns (one for each material) were constructed, consisting of five blocks. The bottoms of the columns were submerged in water. An important step was the scheduling of a periodic replenishment of water to have the blocks always wet at their base. The three columns were weighed periodically, the amount of water collected was evaluated, and a thermographic survey was performed. To quantify the level of the induced disturbance, it was proposed to proceed with three more columns, consisting of the same materials, taken at the same time from the same quarry, but not undergoing the process of disassembly and reassembly, which follow the same wetting process as the first columns. In this way, by comparing the thermographs between the weighted and unweighted columns, it is possible to get a qualitative idea of what the perturbation induced by weighing may have been.

The innovativeness of the proposed method is to use multiblock columns that can be “disassembled” to proceed with a periodic weighing of the individual blocks. The objective is to proceed as quickly as possible and to disrupt the phenomenon as little as possible.

In addition, thanks to a preliminary investigation of the composition and structure of the stones, it was possible to contextualize the data obtained from the monitoring proposed by the protocol. In fact, each stone was characterized in the laboratory by measuring the porosity imbibition, drying index, permeability, capillarity, and sorptivity. This provided support to all the results obtained.

The mesopores present in the tuff facilitate capillary rise phenomena, while the low increase in weight of carparo is due to the high percentage of macropores that do not facilitate capillary rise. In Lecce stone, as in tuff, there is an initial increase in weight, whereas, in tuff, the increase is almost instantaneous, in Lecce stone it is protracted in time. This is due to the presence of very small pores inside the Lecce stone. In general, the smaller the capillaries, the more they tend to absorb moisture and retain it. The same very thin capillaries, however, significantly hinder the movement of moisture within them, making it very slow. For each material, at the end of the experimental test, the following final values of ascent height were recorded: about 21 cm for carparo, about 40 cm for Lecce stone, and 43 cm for tuff.

The protocol allows for easy mapping of rising water for effective retrofit solutions, which without careful observation, could be ineffective. The proposed method is easy to apply and offers a clear methodology within a well-defined time frame. It can be adapted to other types of stone or building materials.

**Author Contributions:** Conceptualization, P.M.C. and C.B.; methodology, P.M.C. and C.B.; formal analysis, P.M.C., C.B., G.Q. and P.D.G.; investigation, P.M.C., C.B., G.Q. and P.D.G.; resources, P.M.C.; data curation, P.M.C. and C.B.; writing—original draft preparation, C.B. and D.D.; writing—review and editing, C.B. and D.D.; visualization, P.M.C. and C.B.; supervision, P.M.C. and C.B. All authors have read and agreed to the published version of the manuscript.

**Funding:** This research received no external funding.

**Institutional Review Board Statement:** Not applicable.

**Informed Consent Statement:** Not applicable.

**Data Availability Statement:** Not applicable.

**Conflicts of Interest:** The authors declare no conflict of interest.

## Appendix A

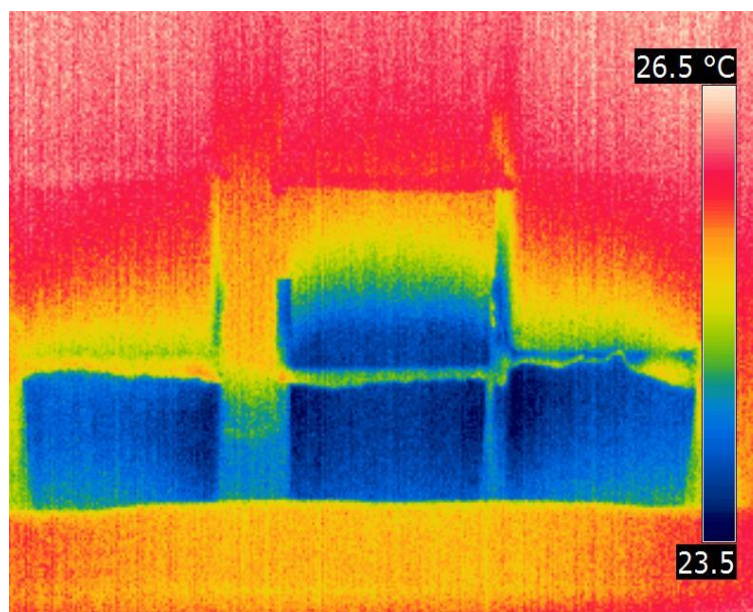


**Figure A1.** Thermographic report dated 21 September 2018, for Carparo (C.), Lecce stone (L.S.), and Tuff (T).

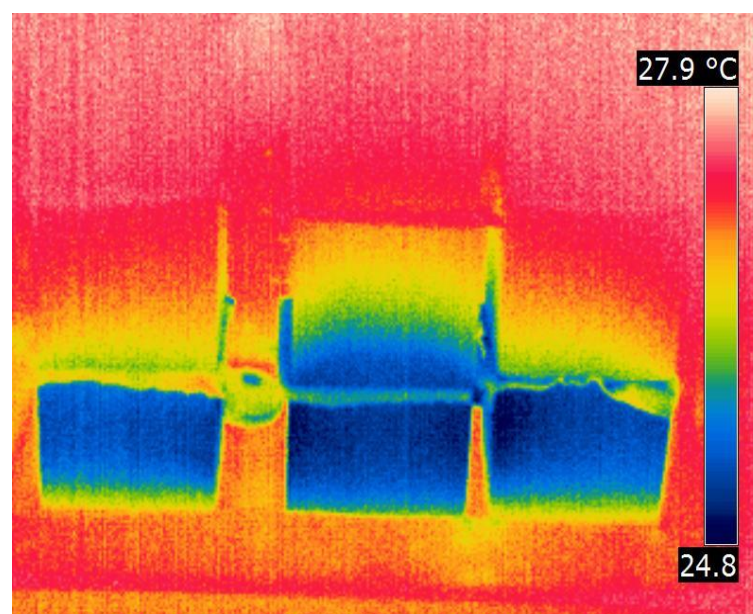


**Figure A2.** Thermographic report dated 28 September 2018, for Carparo (C.), Lecce stone (L.S.), and Tuff (T).

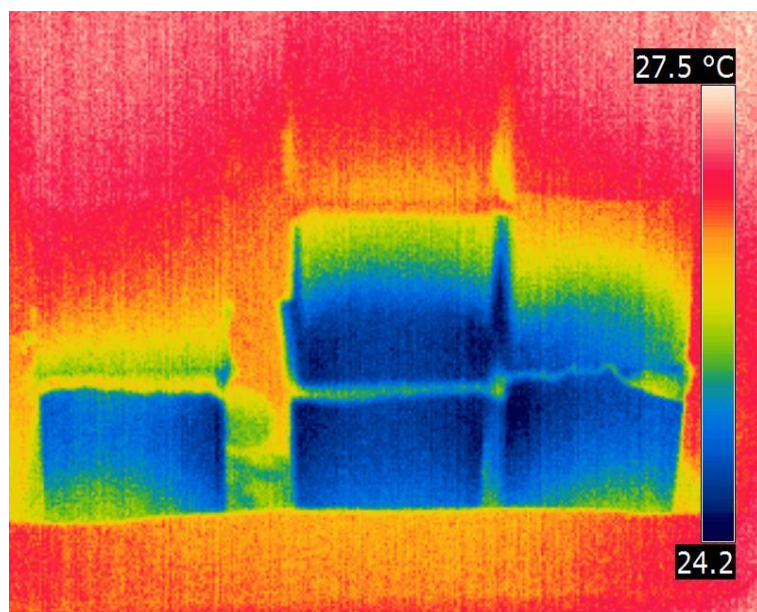


**Figure A3.** Thermographic report dated 5 October 2018, for Carparo (C.), Lecce stone (L.S.), and Tuff (T.).

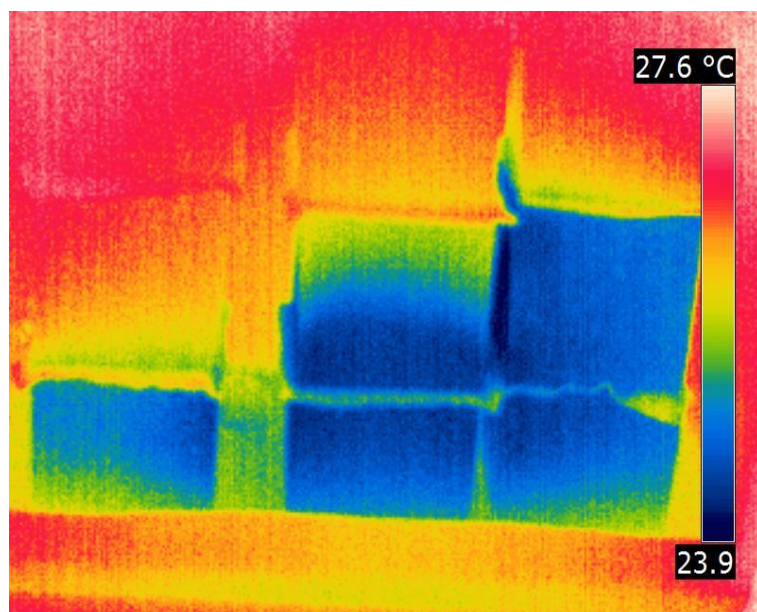


**Figure A4.** Thermographic report dated 12 October 2018, for Carparo (C.), Lecce stone (L.S.), and Tuff (T.).

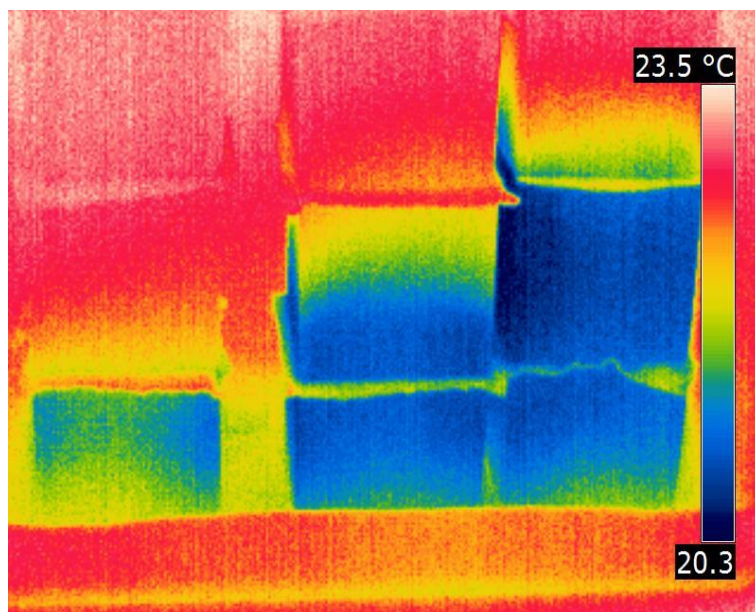


**Figure A5.** Thermographic report dated 26 October 2018, for Carparo (C.), Lecce stone (L.S.), and Tuff (T.).

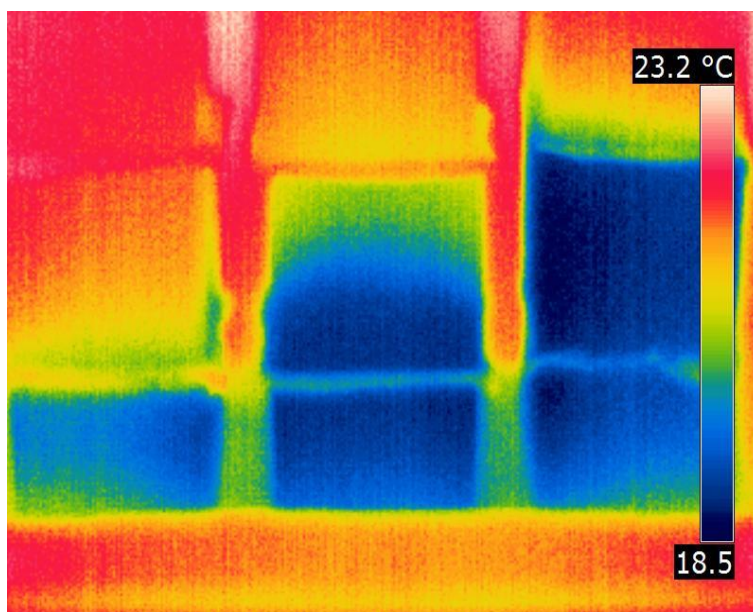


**Figure A6.** Thermographic report dated 9 November 2018, for Carparo (C.), Lecce stone (L.S.), and Tuff (T.).

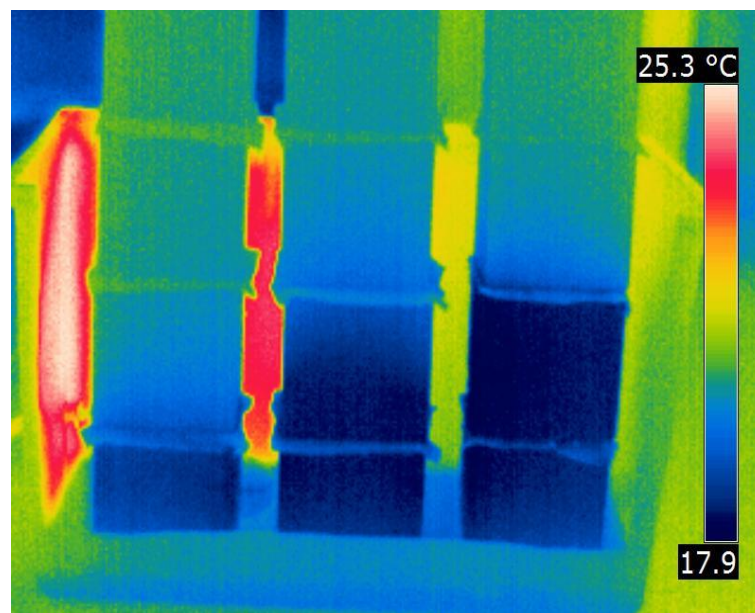


**Figure A7.** Thermographic report dated 23 November 2018, for Carparo (C.), Lecce stone (L.S.), and Tuff (T.).

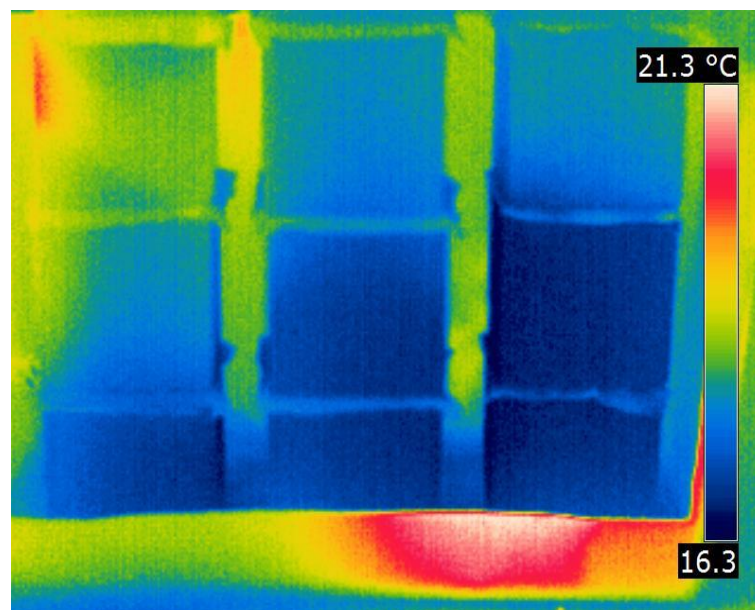


**Figure A8.** Thermographic report dated 7 December 2018, for Carparo (C.), Lecce stone (L.S.), and Tuff (T.).

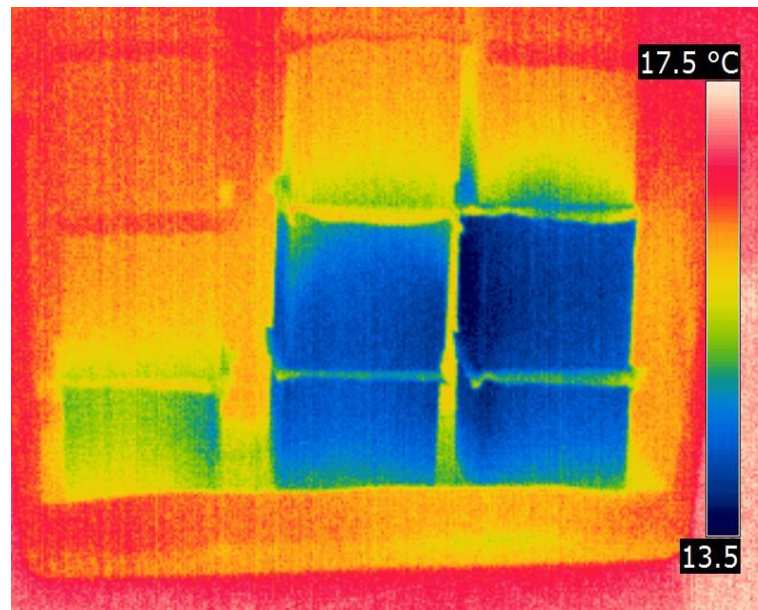


**Figure A9.** Thermographic report dated 21 December 2018, for Carparo (C.), Lecce stone (L.S.), and Tuff (T).

## References

- Hong, T.; Koo, C.; Kim, J.; Lee, M.; Jeong, K. A review on sustainable construction management strategies for monitoring, diagnosing, and retrofitting the building's dynamic energy performance: Focused on the operation and maintenance phase. *Appl. Energy* **2015**, *155*, 671–707. [[CrossRef](#)]
- Prieto, A.J.; Verichev, K.; Silva, A.; de Brito, J. On the impacts of climate change on the functional deterioration of heritage buildings in South Chile. *Build. Environ.* **2020**, *183*, 107138. [[CrossRef](#)]
- D'Agostino, D.; Zacà, I.; Baglivo, C.; Congedo, P.M. Economic and Thermal Evaluation of Different Uses of an Existing Structure in a Warm Climate. *Energies* **2017**, *10*, 658. [[CrossRef](#)]
- Congedo, P.M.; Baglivo, C.; Seyhan, A.K.; Marchetti, R. Worldwide dynamic predictive analysis of building performance under long-term climate change conditions. *J. Build. Eng.* **2021**, *42*, 103057. [[CrossRef](#)]
- Malvoni, M.; Baglivo, C.; Congedo, P.M.; Laforgia, D. CFD modeling to evaluate the thermal performances of window frames in accordance with the ISO 10077. *Energy* **2016**, *111*, 430–438. [[CrossRef](#)]
- Congedo, P.M.; Baglivo, C.; D'Agostino, D.; Quarta, G.; Di Gloria, P. Rising damp in building stones: Numerical and experimental comparison in lecce stone and carparo under controlled microclimatic conditions. *Constr. Build. Mater.* **2021**, *296*, 123713. [[CrossRef](#)]
- D'Agostino, D. Moisture dynamics in an historical masonry structure: The Cathedral of Lecce (South Italy). *Build. Environ.* **2013**, *63*, 122–133. [[CrossRef](#)]
- Franzen, C.; Mirwald, P.W. Moisture sorption behaviour of salt mixtures in porous stone. *Geochemistry* **2008**, *69*, 91–98. [[CrossRef](#)]
- Castelluccio, R.; Vitiello, V. *Il Risanamento Delle Murature Affette da Umidità da Risalita Capillare—Il Metodo CNT*; Luciano Editore: Napoli, Italy, 2019; pp. 3–4, 9–10, 12–16.
- Sawdy, A.; Price, C. Salt damage at Cleeve Abbey, England: Part I: A comparison of theoretical predictions and practical observations. *J. Cult. Herit.* **2005**, *6*, 125–135. [[CrossRef](#)]
- Hall, C.; Hoff, W.D. *Water Transport in Brick, Stone and Concrete*; Taylor & Francis: London, UK; New York, NY, USA, 2002; ISBN 0-419-22890-X.
- O'Brien, P.F.; Bell, E.; Santamaria, S.P.; Boyland, P.; Cooper, T.P. Role of mortars in the decay of granite. *Sci. Total Environ.* **1995**, *167*, 103–110. [[CrossRef](#)]
- Moreno, F.; Vilela, S.A.G.; Antunes, Â.S.G.; Alves, C.A.S. Capillary-rising salt pollution and granitic stone erosive decay in the parish church of Torre de Moncorvo (NE Portugal)-implications for conservation strategy. *J. Cult. Herit.* **2006**, *7*, 56–66. [[CrossRef](#)]
- Amoroso, G.; Fassina, V. *Stone Decay and Conservation-Atmospheric Pollution, Cleaning, Consolidation and Protection*; Elsevier: Amsterdam, The Netherlands, 1893.
- Y'Anson, S.J.; Hoff, W.D. Water movement in porous building materials—VIII. Effects of evaporative drying on height of capillary rise equilibrium in walls. *Build. Environ.* **1986**, *21*, 195–200. [[CrossRef](#)]
- Baglivo, C.; Congedo, P.M. Optimization of high efficiency slab-on-ground floor by multi-objective analysis for zero energy buildings in mediterranean climate. *J. Build. Eng.* **2019**, *24*, 100733. [[CrossRef](#)]

17. Baglivo, C.; Congedo, P.M.; Sassi, V. Numerical dataset of slab-on-ground floor for buildings in warm climate from a multi-criteria analysis. *Data Brief* **2018**, *20*, 269–276. [[CrossRef](#)]
18. Torres, M.I.M.; de Freitas, V.P. Treatment of rising damp in historical buildings: Wall base ventilation. *Build. Environ.* **2007**, *42*, 424–435. [[CrossRef](#)]
19. D’Agostino, D.; Congedo, P.M.; Cataldo, R. Computational fluid dynamics (CFD) modeling of microclimate for salts crystallization control and artworks conservation. *J. Cult. Herit.* **2014**, *15*, 448–457. [[CrossRef](#)]
20. D’Agostino, D.; Congedo, P.M. CFD modeling and moisture dynamics implications of ventilation scenarios in historical buildings. *Build. Environ.* **2014**, *79*, 181–193. [[CrossRef](#)]
21. D’Agostino, D.; Macchia, A.; Cataldo, R.; Campanella, L.; Campbell, A. Microclimate and salt crystallization in the crypt of lecces Duomo. *Int. J. Archit. Herit.* **2015**, *9*, 290–299. [[CrossRef](#)]
22. Snethlage, R.; Wendler, E. Moisture cycles and stone degradation. In *Saving Our Cultural Heritage. The Conservation of Historic Stone Structures*; Baer, N.S., Snethlage, R., Eds.; John Wiley and Sons: Chichester, UK, 1996; pp. 7–24.
23. Straube, J.; Burnett, E.F.P. Overview of hygrothermal (HAM) analysis methods. In *ASTM Manual 40—Moisture Analysis and Condensation Control in Building Envelopes*; Trechsel, H.R., Ed.; ASTM: West Conshohocken, PA, USA, 1991; Chapter 5; pp. 81–89.
24. UNI EN 13755: 2008. *Natural Stone Test Methods—Determination of Water Absorption at Atmospheric Pressure*; CEN: Brussels, Belgium, 2008.
25. UNI EN 16322: 2013. *Conservation of Cultural Heritage-Test methods-Determination of Drying Properties*; UNI: Milan, Italy, 2013.
26. Normal 21/85: Permeabilità del Vapor d’acqua”, Part of the “Raccomandazioni Normal: Alterazioni dei Materiali Lapidari e Trattamenti Conservativi: Proposte per L’unificazione dei Metodi Sperimentali di Studio e di Controllo”. Available online: <http://www.urbis-libnet.org/vufind/Record/ICCROM.ICCROM49201/Details> (accessed on 10 December 2021).
27. UNI EN 15801: 2009. *Conservation of Cultural Property-Test Methods-Determination of Water Absorption by Capillarity*; UNI: Milan, Italy, 2009.
28. Sharpe, R.W. A mortar for rising damp studies. *Build. Environ.* **1978**, *13*, 261–265. [[CrossRef](#)]
29. Vasovic, D.; Terzovic, J.; Kotic, A.; Okrajnov-Bajic, R.; Sekularac, N. The Influence of Water/Binder Ratio on the Mechanical Properties of Lime-Based Mortars with White Portland Cement. *Crystals* **2021**, *11*, 958. [[CrossRef](#)]
30. Acquedotto Pugliese, Durezza Dell’acqua. Available online: <http://majorana.weebly.com/files/theme/DurezzaAcqua.pdf> (accessed on 10 December 2021).